



## ESTIMATING LOSSES DUE TO A RECURRENCE OF THE 1960 M9.5 MEGATHRUST EARTHQUAKE IN SOUTHERN CHILE

A. Nasser<sup>(1)</sup>, A. Farias<sup>(2)</sup>, T. Lai<sup>(3)</sup>, M. Turel<sup>(4)</sup>, Y. Yin<sup>(5)</sup>, S. Li<sup>(6)</sup>

<sup>(1)</sup> Senior Engineer, Manager, AIR-Worldwide, [anasseri@air-worldwide.com](mailto:anasseri@air-worldwide.com)

<sup>(2)</sup> Engineer, AIR-Worldwide, [afariasvelasco@air-worldwide.com](mailto:afariasvelasco@air-worldwide.com)

<sup>(3)</sup> AVP Senior Principle Engineer, AIR-Worldwide, [tlai@air-worldwide.com](mailto:tlai@air-worldwide.com)

<sup>(4)</sup> Senior Scientist, Chubb, [mesut.turel@chubb.com](mailto:mesut.turel@chubb.com)

<sup>(5)</sup> Senior Engineer, AIR-Worldwide, [yvin@air-worldwide.com](mailto:yvin@air-worldwide.com)

<sup>(6)</sup> Senior Engineer, AIR-Worldwide, [sli@air-worldwide.com](mailto:sli@air-worldwide.com)

### **Abstract**

Understanding the risk due to natural and man-made catastrophes is one of the primary steps in evaluating the capacity of a community to manage disasters and in creating resilience. In seismic prone regions, the need for estimating possible losses due to future earthquakes has long been recognized by emergency planners, financial organizations and the insurance industry. This study presents an application of the AIR earthquake model for South America in estimating possible losses from a recurrence of the 1960, M9.5 earthquake in Chile which also spawned a large tsunami. In Chile, the earthquake and tsunami caused extensive damage in the coastal area and in particular in the city of Valdivia. The economic loss from this event has been estimated between \$250 and \$1,500 million USD in 1960 values. Considering the significant growth in population and urbanization as well as advancement in engineering and construction, this paper provides an estimate of possible direct losses due to shaking, liquefaction, and tsunami for building properties (excluding infrastructure) using a high resolution (1km by 1km grid) database of the current building inventory. It is shown that the total direct losses not including business interruption can be as large as 16.2 trillion CLP (~USD \$29b).

*Keywords: loss estimation, tsunami simulation, megathrust earthquake*



## 1. Introduction

A catastrophic event, such as an earthquake or a hurricane, can disrupt a nation's economic and social integrity. While natural disasters cannot be avoided, their impact can be assessed and mitigated. Understanding the hazard and vulnerability of an urban society to catastrophes is the primary step in evaluating its capacity to manage disasters and to carry out an efficient recovery when such an event happens. In some seismic prone regions, the need for estimating possible losses due to future earthquakes has long been recognized by emergency planners, financial organizations and (re)insurance companies. AIR-Worldwide has developed earthquake loss estimation models for a number of countries around the globe (including five countries in South America) in which regional hazard and vulnerability modules are used to evaluate the risk posed to inventories of exposed property. Through probabilistic seismic analysis, these models provide a basis for the aforementioned organization to make informed decisions in managing their risk.

Chile is located in the Pacific Coast of South America along the so-called "ring of fire" which has produces many of the world's most devastating earthquakes. Seismicity in Chile is characterized by large magnitude earthquakes generated by the subduction of the Nazca plate under the South American plate. In recent years the M8.8 Maule earthquake in 2010, the M8.1 Iquique earthquake in 2014 and the M8.3 Illapel event in in 2015 demonstrated the threat of earthquakes in Chile. In 1960 a magnitude 9.5 earthquake - the largest earthquake ever recorded - occurred off the coast of Chile near Valdivia [1]. The 1960 earthquake generated a large tsunami and caused extreme devastation throughout Chile. Tsunami waves battered the Chilean coast and traversed the Pacific Ocean causing damage as far as Hawaii and Japan. The economic loss from this event in Chile has been estimated between \$250 and \$1,500 million USD in 1960 values.

In a few decades after the 1960 earthquake, Chile has seen an increase in urbanization and development. Considering the particular shape of the country with rather narrow E-W extent, much of Chile is subjected to high seismicity from subduction zone earthquakes. The combination of high seismic hazard and exposure concentration along the coast relatively close to the source of these subduction zone earthquakes has rendered this a high-risk region for financial organizations and the government. This paper presents an application of the AIR earthquake model for a scenario analysis in Chile to estimate the potential losses to building properties in Chile from a recurrence of the 1960 earthquake.

The scenario simulation presented here provides estimates of potential direct losses caused by shaking, tsunami, and liquefaction using a high-resolution (1km by 1km) property inventory database. Loss estimates reported in this paper reflect losses from damage to building and contents, but do not include losses due to business interruption. Maps showing the distribution and size of losses illustrate the impact of the event in the region. The next sections provide a brief description of seismic hazard in Chile, the selected scenario, the components of the model and the results of the study.

## 2. Seismicity in Chile and the 1960 M9.5 earthquake

Chile is located on the South American plate near its boundary with the Antarctic and Nazca plates. Both the Nazca and Antarctic plates subduct beneath the South American plate. The Nazca plate moves east a rate of approximately 80 mm per year with respect to the South American plate, while the Antarctic plate moves to the east at a rate of 20 mm per year. North of 46°S latitude, the seismicity in Chile is primarily driven by the activity of the Nazca plate, whose subduction has produced the Andes Mountains. South of the 46°S latitude, seismicity is mainly driven by the movement of the Antarctic and South American plates. Fig. 1 shows the tectonic setting and the historical seismicity in South America.

The majority of earthquakes in South America take place in subduction zones with the depths of these events varying widely. Shallow events occur at a depth of less than 70 km, intermediate events occur at depths of 70-300 km, and deep events occur at depths greater than 300 km. Shallow earthquakes are generally concentrated along trenches which frequently generate strong events. During the twentieth century magnitude 8.0 and greater earthquakes have occurred at least once per decade in the Andean Trench.



Fig. 1 – Tectonic context and historical seismicity in South America

The largest magnitude earthquake ever recorded, a M9.5 earthquake near Valdivia, occurred as a shallow earthquake along the Andean Trench on May 22, 1960. Over 1609 km (1000 mi) of fault ruptured along the subduction zone at the interface of the Nazca and South American plates. The earthquake epicenter was located about 700 km (435 mi) south of Santiago, and the focal depth was approximately 33 km (20 mi). This massive earthquake was accompanied by four foreshocks and five aftershocks that were of magnitude 7.0 and greater.

The Valdivía earthquake caused extreme devastation throughout Chile, particularly along the coast from Concepción to Isla Chiloe. The town of Puerto Montt was devastated, and the village of Toltén was nearly completely reduced to rubble. Major flooding and disruption in telecommunications services hampered rescue and recovery efforts. Nearly 2,000 people lost their lives and 3,000 people were injured. The event left approximately 350,000 people homeless after 145,000 homes were destroyed or damaged. This earthquake spawned localized tsunami waves that battered the Chilean coast. One massive wave crossed the Pacific Ocean and struck Hilo, Hawaii; other waves were recorded as far away as Japan and the Philippines with heights reaching up to 11.5 meters (38 ft) tall [2,3].

## 2.1. Ground motion simulation and local intensity calculation

The first step in estimating damage and losses from this scenario is to determine ground motion intensity parameters such as peak ground acceleration (PGA) and spectral acceleration (at various periods) at all locations where damageable property exists. Once the source parameters of the earthquake are defined, calculation of local intensity follows from the application of ground motion prediction equations (GMPE) or attenuation relationships. The GMPEs provide ground motion intensity as a function of the magnitude, distance, and rupture mechanism of the earthquake.

GMPEs are developed empirically using ground motion data from earthquakes with certain fault mechanism in different region. However, due to the lack of ground motion recordings for subduction earthquakes, most GMPEs for earthquakes with this particular type of rupture mechanism are developed using data collected from around the world. The GMPEs used in the AIR model for subduction zones generally reflect those used by the USGS, the Geological Survey of Canada, and HERP Japan. However, in Chile, most of the recorded ground motions from large earthquakes on the Nazca subduction zone exhibit a characteristically stronger level of shaking than those predicted using the global GMPEs developed for other similar tectonic



environments. Using the ground motion records from thirteen Chilean subduction zone earthquakes, including some records from the 2010 Maule M8.8 earthquake, Contreras and Boroschek [4] developed a Nazca-specific GMPE for interface earthquakes. This GMPE is considered to be the most representative GMPE for interface earthquakes in the region; thus, a higher weighting factor is applied to Contreras and Boroschek GMPE than to the global GMPEs including Youngs et al. 1997 [5], Atkinson and Boore, 2003 [6], Zhao et al. 2006 [7], and Gregor et al. 2002 [8].

The shaking intensity that a structure experiences at any given location is significantly affected by local soil type and site conditions. In earthquake simulations the impact of site condition is addressed through site amplification factors for different soil types (e.g. by NEHRP classification). The AIR Earthquake Model for Chile employs the latest high resolution geological maps and microzonation studies that capture high-resolution variations in local site conditions in order to provide realistic site amplification estimates for ground motion prediction. Specifically, microzonation reports available for Concepción [9], Santiago [10,11], San Pedro [12], and San Antonio [13] were used. Fig. 2 shows the simulated footprint of the peak ground acceleration for the considered scenario using the median ground motion obtained from the GMPEs. The largest PGA is estimated at 0.5g.

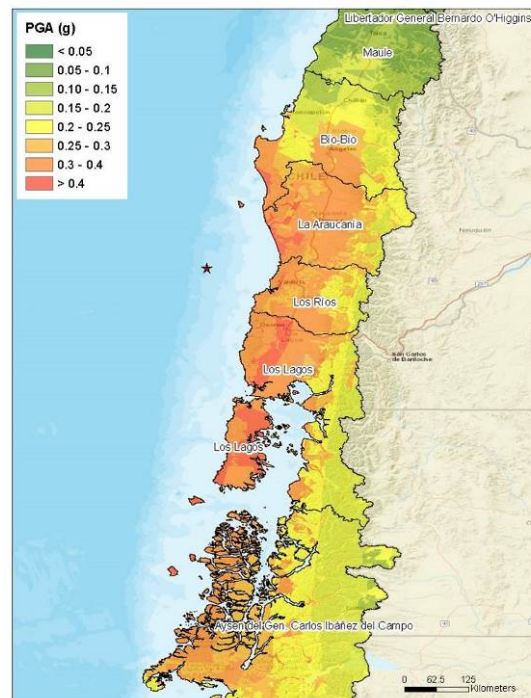


Fig. 2 – Peak ground acceleration footprint for the simulated M9.5 event

## 2.2. Tsunami simulation

A separate simulation is carried out to model the impact of a massive tsunami that was generated by this earthquake. The AIR Earthquake Model for South America employs a modified version of TUNAMI (Tōhoku University's Numerical Analysis Model for Investigation of Near-field Tsunamis) [14] to perform tsunami simulations. It is a 2-D shallow water numerical grid-point model capable of simulating the propagation of a tsunami and modeling the inland extent of water. The size and the impact of the tsunami are determined by the characteristics of the fault (location, width of the fault plane, dip angle, and focal depth) and its subsequent rupture (slip distribution on the rupture plane). The model generates an initial displacement of the water surface and uses the method of deformation of an elastic half-sphere [15] to solve the mass and momentum equations of motion at specified time steps on an array of grid points using a finite difference methodology. Close to the shore, the effects of friction via a Manning coefficient are used to limit inundation. To achieve a balance

between computation time and accuracy the model uses a nested domain with varying resolution. In the open ocean away from the coast, the model resolution is coarser; resolution of the domain increases to a max of 132 meter resolution closer to the shore.

Modification to the original TUNAMI model enables explicit consideration for levees and their probabilistic failure as well as the influence of spatially varying astronomical tides. The model provides inundation height and flow velocity at user-specified time intervals. The maximum inundation height and flow velocity are the two parameters that are used in estimating the damage to property due to the tsunami waves.

Fig. 3 shows the maximum inundation height (above the ground surface) for the areas that experienced the highest impact from the tsunami. Around Puerto Saavedra (right figure) the model shows a tsunami height of 9-12 meters. The model also shows that water penetrates about 3-5 kilometers inland. Farther south in the coastal area near Toltén, the modeled tsunami height is about 12-14 meters. A few kilometers inland, the inundation height in Nueva Toltén is estimated about 1.5-2 meters. The left panel of Fig. 3 shows inundation height around Concepción. In some coastal areas north of Concepción (e.g. Talcahuano) the model estimates a water depth of 2-5 meters. The modeled inundation height matches the account of various sources for the 1960 earthquake that reported about 11.5 meters of inundation in Puerto Saavedra and severe damage in Toltén and Corral.

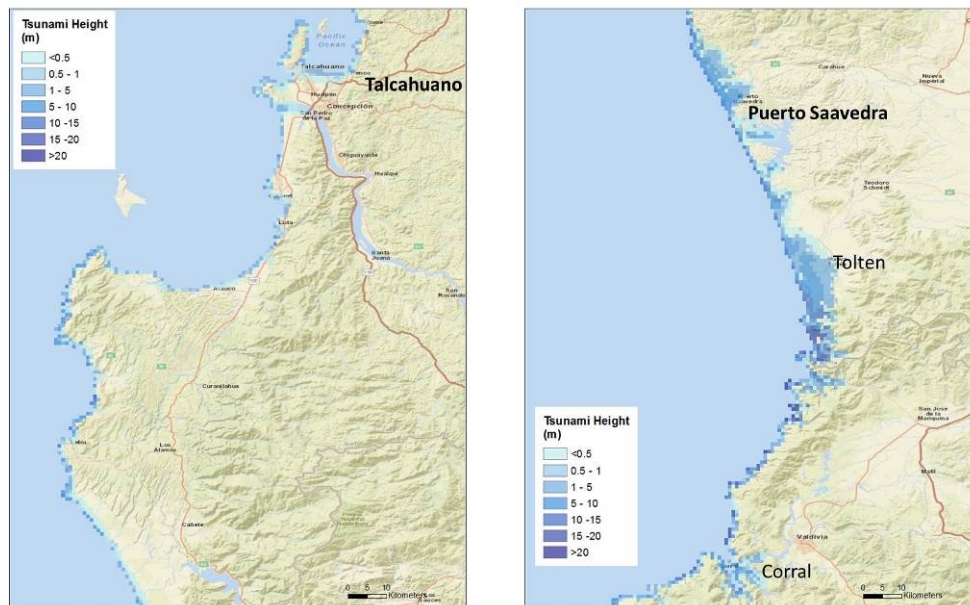


Fig. 3 – Tsunami inundation height

### 3. Exposure at risk of earthquake damage

Since the 1960 earthquake, Chile has experienced significant growth and urbanization. Statistical analysis of GDP data and new building data available from 1991 onwards from Instituto Nacional de Estadística (INE) [16] suggests that about 40-50% of Chile's current building inventory was built between 1994 and 2010. To present a realistic picture of the consequence of a recurrence of this earthquake in Chile today, it is crucial to have a reliable estimate of the exposure at risk. An essential part of the AIR loss estimation models is a database containing the inventory of the properties at risk and an estimate of their replacement value. To compile the building inventory, detailed data (building counts and structure, occupancy, and height classifications) are gathered from a host of sources including municipal and private entities.

Most of the exposure in Chile is concentrated around Santiago, the capital city and the financial center of Chile. However, a significant amount of exposure is concentrated around Valparaíso and San Antonio as well. Today, the majority of residential buildings in urban areas of Chile are of masonry (reinforced masonry, confined masonry or unreinforced masonry) type [17]. Wood and reinforced concrete construction types are also



common. In rural areas most of the residential buildings are constructed of adobe or unreinforced masonry. Commercial buildings are primarily constructed of masonry, concrete, or steel construction. Reinforced concrete shear wall and reinforced masonry construction are both typical of commercial buildings and mid-to-highrise apartment buildings in Chile. Industrial buildings are typically built of steel or light metal construction.

It is important to note that in the context of regional loss estimation, it is not practical to analyze every individual building. To keep the size and resolution of the analysis to a manageable scale it is necessary to group the exposures in some reasonable geographical and typological classifications. In this study buildings are classified based on their construction material, structural system, occupancy, and building height with the exposure spatially distributed at a resolution of 1km by 1km. The exposure used in this study contains building assets of various occupancies, but does not account for the infrastructure and lifeline systems. In valuation of the exposure, structural and non-structural building components as well as the contents of the buildings are taken into account.

#### 4. Seismic vulnerability module

Vulnerability functions provide a relationship between hazard intensity and expected damage which is defined as the ratio of repair cost to replacement value. To provide comprehensive damage estimation, the AIR model accounts for earthquake damage due to shaking as well as the accompanying perils of tsunami and liquefaction. In developing damage functions, buildings are typically grouped into different “construction types” defined by material and structural systems. Damage functions are developed for each construction type and height (lowrise, midrise and highrise) rather than for individual buildings. They are commonly developed based on expert opinion, observational data, analytical studies, or a combination of these [18]. Observational methods, which rely on the statistical analysis of data from post-earthquake damage surveys, and sometimes insurance claim data, are realistic but limited by the availability of data. Analytical approaches synthesize data for statistical analysis through structural analysis and can overcome the limitations of observational methods with regard to data availability and reliability. However, the accuracy and reliability of these analytical approaches can be limited by modeling capabilities and computational costs. Damage functions in this study are developed with a hybrid approach, using both analytical and observational data to support and supplement both approaches.

##### 4.1. Shake damage

By the virtue of a long history of experiencing large earthquakes, Chile has been on the forefront of establishing and advancing seismic design provisions. Since the publication of the first building code of Chile in 1932, which included seismic design guidelines, both seismic loading codes and material design codes have evolved significantly over time. Consequently, the modeled vulnerability of buildings varies both by location and by the year of construction. The current seismic design code in Chile NCh433 (and the improvements after the 2010 Maule earthquake) requires the same level of stringency as the ASCE-7 code does for seismically active regions in the United States [19].

Shake damage functions used in this study are presented in terms of spectral acceleration at different natural periods ( $S_a(0.3)$  for low-rise,  $S_a(1.0)$  for mid-rise, and  $S_a(2.0)$  for high-rise, and  $S_a(3.0)$  for tall buildings). Nonlinear dynamic analysis (NDA) of numerical models representing each “construction type” subjected to a large ensemble of ground motions is used to establish relationships between engineering demand parameters (EDP), and ground motion intensities. A total of 5679 ground motion records from around the globe obtained from the Pacific Earthquake Engineering Research Center (PEER) database were used in the study to synthesize data for damage function development. Ground motions used in NDA represent a wide range of magnitude ( $M_w$  4.4-7.7), distance, duration, and soil type. The synthesized response data was post-processed through an assembly-based vulnerability assessment by leveraging component-level fragility data from PACT (FEMA P-58, “Performance Assessment Calculation Tool”) [20] to convert the EDP to physical damage and monetary loss. Process of damage function validation is informed by vulnerability studies of other researchers [21, 22, 23] and by observational data from the 2010 Maule earthquake, the 2007 Pisco earthquake in Peru, the



2011 Tohoku in Japan and the 1994 Northridge earthquake for certain construction types for which damage data is available.

To reflect the spatial and temporal variation in vulnerability, similar to the approach used in HAZUS, the vulnerability of buildings of the same type and height is further classified into five levels based on their expected seismic resistance. These vulnerability classes are defined in terms of seismic code levels which reflect the degree of scrutiny used in design and construction of these buildings. Accordingly, damage functions are developed for five vulnerability classes which include “pre-code” (e.g. building with no seismic design), “low-code” (e.g. buildings designed to early version of seismic codes), “moderate-code”, “high-code” and “special-code” (e.g. buildings designed to the most stringent codes in seismically active regions) in descending order of vulnerability. For more information about the uniform vulnerability assessment framework used in this study refer to [24]. Fig. 4(a) shows an example of damage functions for low-rise reinforced concrete (RC) frame structures.

#### 4.2. Tsunami damage

Tsunami damage is caused by a combination of hydrostatic forces (related to water depth), hydrodynamic forces (related to flow velocity), and debris collision and buoyancy forces that wash the buildings away and turn them into new debris. In a broader aspect, tsunami damage can also include soaking, scouring by sand or other sediments against surfaces, sedimentation, and chemical contamination.

Tsunami damage functions in the AIR Earthquake model are developed empirically using a large set of observational data from 1993 Hokkaido, 2004 Indian Ocean, 2010 Maule, and 2011 Tohoku tsunamis. Additionally, studies from Japan’s Ministry of Land, Infrastructure, Transport, and Tourism (MLIT) [25] and Reese et al. (2011) [26] were used to develop relationships between the tsunami inundation and flow velocity in generating the damage functions. The vulnerability functions explicitly account for the hydrostatic, hydrodynamic, and buoyancy forces by taking into account the inundation depth and flow velocity. Other factors such as soaking, scouring, contamination, and sedimentation are implicitly accounted for in the damage estimates as the data used to develop the damage functions include the impact of these sources.

Moreover, the effect of debris on building damage is accounted for through empirically developed debris functions for buildings of different construction type and height. At very shallow depths (<0.5 m), usually there is little to no impact from debris. Increased inundation height intensifies the buoyancy forces causing an increase in the size and quantity of damaging debris. The debris effect increases with inundation only up to a point; it falls off at higher inundation levels where the building is already damaged and the debris do not cause further damage. Fig. 4(b) shows an example of tsunami damage functions for low rise RC buildings.

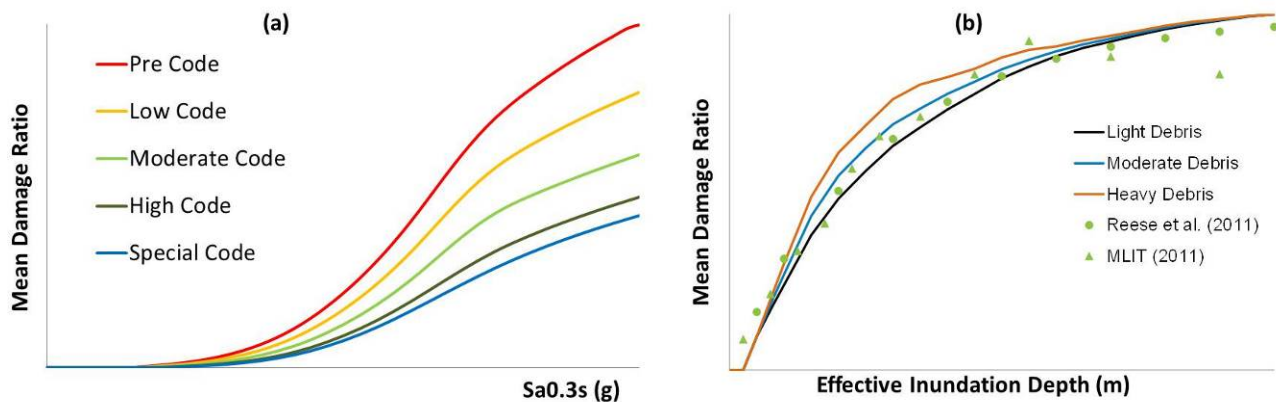


Fig. 4 – Vulnerability functions used in the AIR earthquake model: (a) Example shake damage functions for low rise RC buildings of different vulnerability classes; (b) Tsunami damage functions for low rise RC buildings.



### 4.3. Liquefaction damage

As highlighted by recent earthquakes in New Zealand (2010 and 2011) and in Japan (2011), ground failure can contribute significantly to the overall losses resulting from an earthquake. In a comprehensive loss estimation study it is imperative to include the losses from these perils. Unlike shake damage, which often occurs in a vast area, ground failure is often localized and confined to areas that are prone to the hazard. Estimating losses from ground failure in a regional loss estimation model requires detailed information about the physical properties of the affected area including soil type and ground water depth.

Development of a regional liquefaction module relies on the strong correlation that exists between liquefaction susceptibility and surficial geology. This study uses groundwater depth data obtained from a global water table depth map and a database of bodies of water [27]. Liquefaction hazard and surficial geological maps are obtained from Servicio Nacional de Geología y Minería (SERNAGEOMIN) of Chile and published relationships between surficial geology and liquefaction hazard [28].

The liquefaction estimation method used in this model compares the soil's ability to resist liquefaction to the imposed liquefaction demand, which follows collective research summarized in [29]. Liquefaction resistance is defined by soil strength characterized by shear-wave velocity, soil type, and groundwater depth, while liquefaction demand is a function of ground motion intensity. Building damage resulting from liquefaction is modeled as a function of permanent ground displacement (PGD) due to post-liquefaction reconsolidation settlement. PGD is determined using the relationship between factor of safety and volumetric strain proposed by Ishihara and Yoshimine [30]. Liquefaction vulnerability functions are developed by adopting the HAZUS liquefaction damage calculation methodology and modifying it using damage data from the recent Japan and New Zealand earthquakes.

## 5. Damage and loss estimates

The simulation shows that most of the regions in Chile are impacted by this earthquake scenario with varying degrees of damage. Results of the study are presented in terms of total monetary losses and loss ratios (defined as the aggregated loss divided by the total replacement value) at different geographical resolutions from 1km grids to larger administrative regions. Loss ratio footprints conveniently demonstrate the extent and severity of damage in the affected regions and also show the areas where the tsunami and liquefaction sub-perils may have greater damaging impact. Damage and loss estimates reported here include residential, commercial, and industrial properties but do not include public infrastructure and lifeline systems. Information presented in the form of loss breakdown by peril and region and loss ratio footprints can be used by public safety and financial planners to identify regions that need attention and to make strategic decisions about mitigation and ultimately for repair and reconstruction planning.

### 5.1. Extent and severity of damage

Fig. 5 shows the loss ratios in the most affected areas by aggregating the losses at each 1km grid cells and dividing it by the total affected exposure value in the same grid. The loss ratios represent the degree of damage sustained to the properties in each grid on an average sense. Large damage is expected in Valdivía, Puerto Montt, and Temuco as well as Concepción and many smaller towns around these areas.

The simulation shows widespread damage due to tsunami along the coast of Chile. Damage is particularly severe around Puerto Saavedra and Toltén. Further north Lebu, Coronel, and Talcahuano also experience high degrees of damage. Tsunami damage extends to the north of Concepción and Constitución; some relatively lighter tsunami damage, is expected in areas as far north as Valparaíso and Viña Del Mar. Fig. 6 illustrates the loss ratios from tsunami damage for 1km grid cells in areas around Puerto Saavedra (left), Concepción (middle) and Valparaíso (right).

Liquefaction does not seem to be a major contributor to the total damage. However, in some locations around Concepción and Hualpén in the Bío-Bío region and Valdivía in Los Ríos region as well as Temuco in La

Araucanía, the model estimates that liquefaction damage will occur. The left panel in Fig. 7 shows the liquefaction susceptibility map in the Concepcion - Hualpén area and the right panel shows the loss ratio due to liquefaction from the simulations.

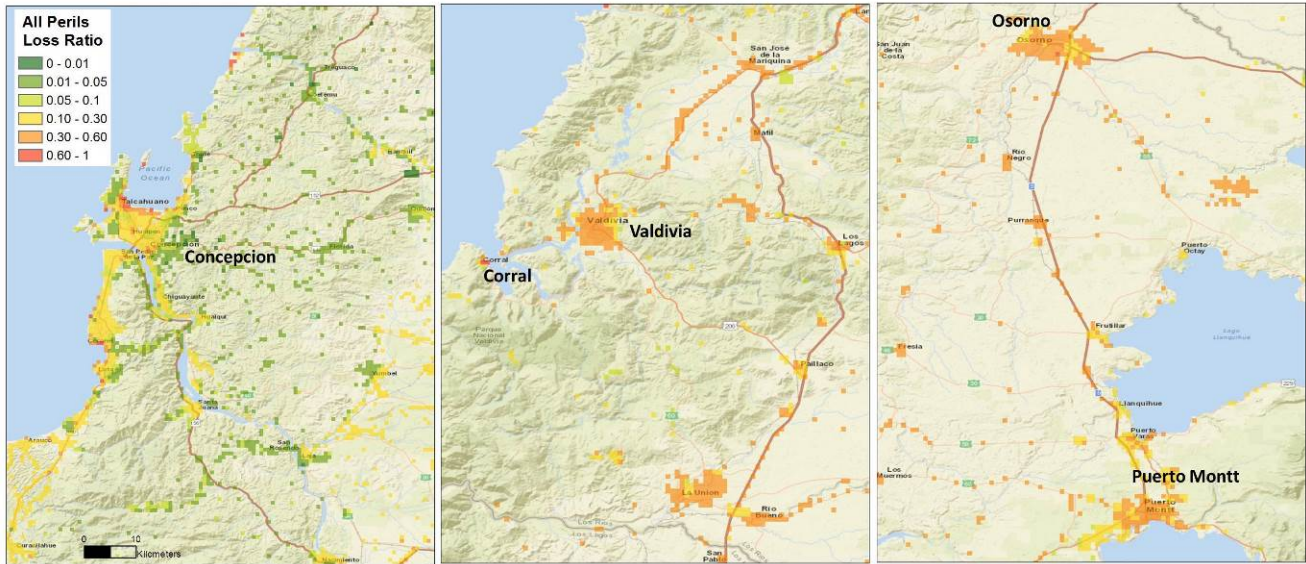


Fig. 5. Loss ratio for damage due to all perils in 1km grid cells for some areas with the largest damage



Fig. 6- Loss ratio for tsunami damage at 1km grid cells

## 5.2. Estimate of direct losses

The model is able to provide an estimate of direct losses from damage to structural and non-structural building components as well as contents in addition to losses incurred by interruption in service. However, the losses values reported in this paper only include direct losses caused by physical damage to building and contents. Table 1 shows the breakdown of losses by peril and by type of property (known as lines of business in the insurance industry).

The direct loss to all properties is estimated at 16.2 trillion CLP (approximately USD \$29b) for the exposure values in 2014. As can be seen in Table 1, despite the large tsunami, losses are dominated by shake

damage. For residential buildings, the contribution of tsunami and liquefaction to the total residential losses are 5.3% and 0.9% respectively. For commercial and industrial buildings the tsunami and liquefaction contributions are 10.2% and 0.7% respectively.

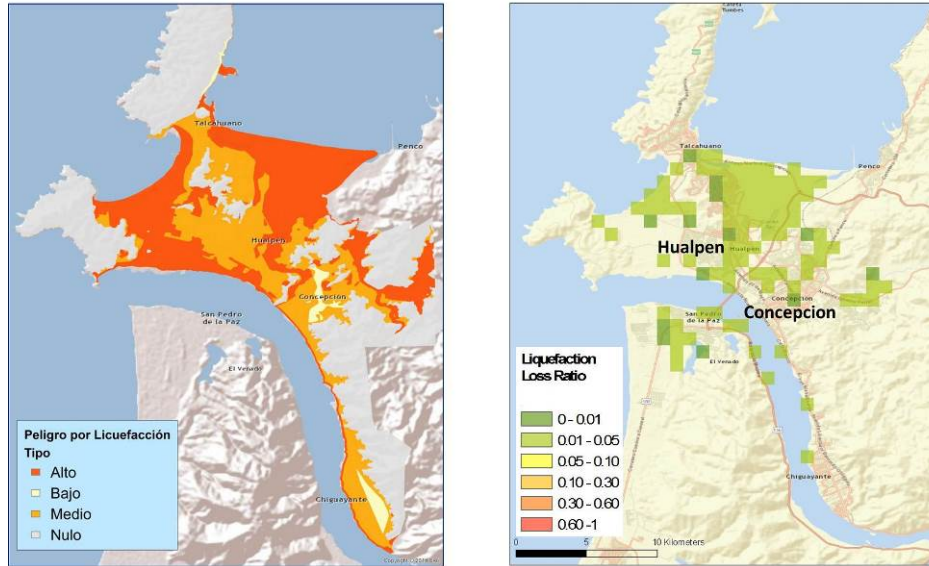


Fig. 7 – Left: liquefaction susceptibility map. Right: Loss ratio for liquefaction at 1km grid cells

Table 1 – Estimated losses by peril for different properties

Type of property	Loss (in million CLP)*			Total
	Shake	Tsunami	Liquefaction	
Residential	6,909,827	392,127	67,013	7,368,968
Commercial/Industrial	7,713,247	883,468	61,298	8,658,013
Automobiles	85,357	58,575	1,792	145,725
<b>Total</b>	<b>14,708,432</b>	<b>1,334,170</b>	<b>130,104</b>	<b>16,172,705</b>

\* Losses reflect damage to buildings and contents and do not include losses due to business interruption.

As shown by the intensity footprint in Fig. 2, the earthquake impact is widespread; 13 out of the 15 administrative regions of Chile experience some level of damage. More than 92% of the total losses occur in Regions VIII (Bío-Bío), IX (La Arucanía), X (Los Lagos) and XIV (Los Ríos). As shown in the left panel of Fig. 8, losses in region VIII constitute 37% of the total loss (6.08 trillion CLP). Severity of damage, represented by loss ratio, varies in these regions. The right panel in Fig. 8 shows the loss ratio in the regions with the highest total losses. Regions IX (La Arucanía) and X (Los Lagos) suffer the heaviest damage. In region IX, which includes some of the hardest hit cities, the loss ratio is as high as 27%.

Administrative regions in Chile are large areas. In order to better understand the distribution of damage and loss within each region, loss ratios are also calculated at the “comuna” (municipality) level which is the smallest administrative subdivision in Chile. Fig. 9 shows loss ratios aggregated at “comuna” level. In the region of La Arucanía, loss ratios in the comunas of Temuco and Cholcol reach 30%. As shown in the inset, loss ratios in the coastal areas are higher owing to the additional severe damage due to tsunami. In Saavedra the loss ratio reaches 58% and in Toltén tsunami destruction has led to large loss ratios as high as 70% for the entire comuna. In Los Ríos region, the loss ratio in Valdivía comuna is about 30% and in the loss ratio is as high as 50% in Coral due to extensive tsunami damage.

It is worth reiterating that the majority of the exposure in Chile is concentrated around Santiago which was neither heavily affected by the 1960 event nor significantly impacted by the simulation discussed in this paper. In the regions that suffer the largest loss the exposure is rather sparse, however almost all of the exposure is

affected by the earthquake. The large loss ratio in some comunas is due to the fact that most of the exposure in the comuna is in the inundated areas or in the areas of high shaking intensity.

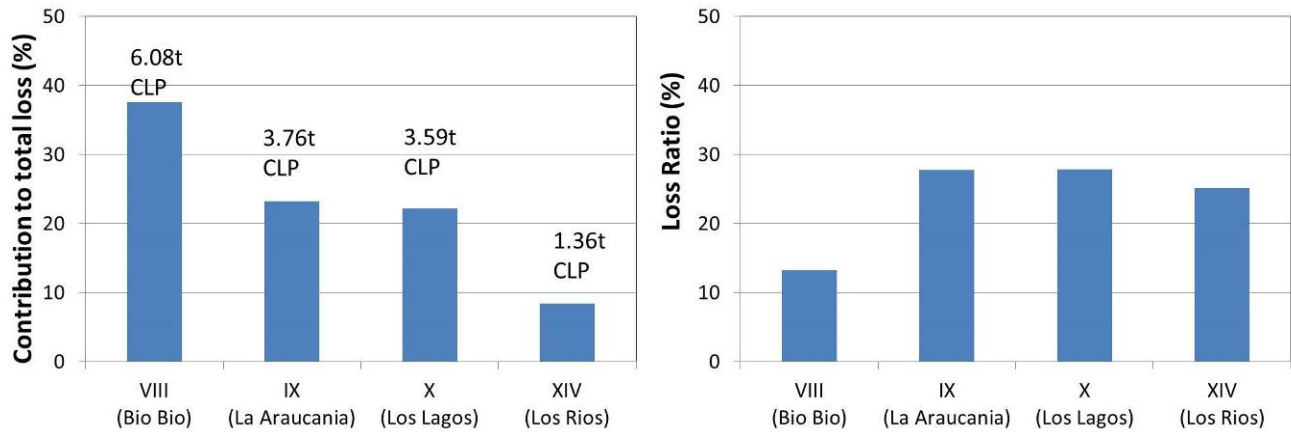


Fig. 8 – Regions with the highest impact. Left: contribution to the total loss. Right: aggregated loss ratio

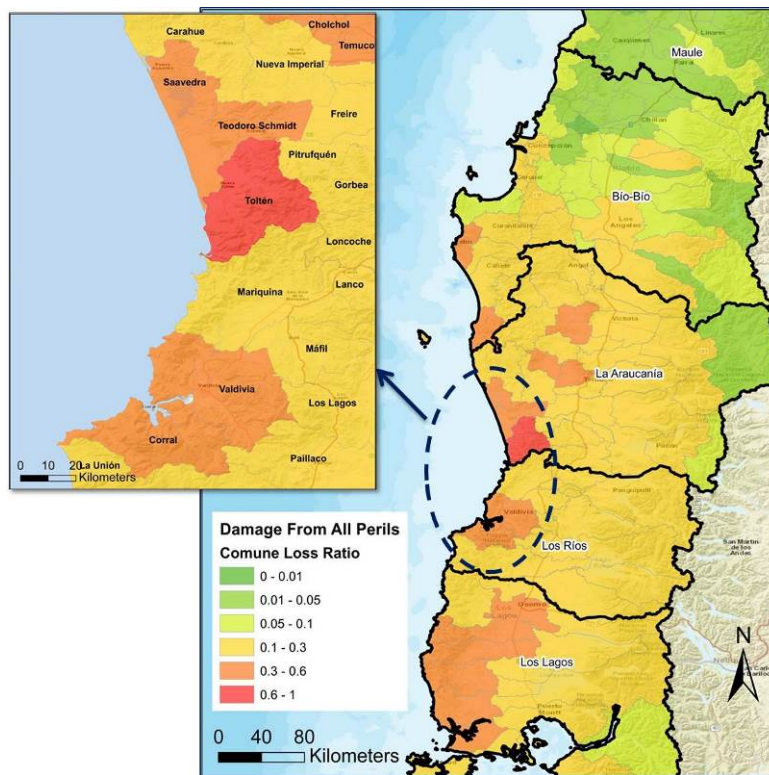


Fig. 9 – Loss ratio due to shake, tsunami and liquefaction at “commune” level

## 6. Conclusions

The study reported here presents an estimation of damage and losses due to a recurrence of the 1960 M9.5 earthquake off the coast of Chile. The magnitude 9.5 event- the largest recorded earthquake in history- triggers a large tsunami and causes ground failure. Although not a prediction of any future event, the results shown in this study provide a picture of the possible impact that such an event can have in different regions of Chile. Simulations show widespread damage due to the combination of shake, tsunami, and liquefaction along the coast with the heaviest damage in the areas Valdivía, Puerto Saavedra and Nueva Toltén. The total direct loss due to



building and content damage is estimated at 16.2 trillion CLP (~ USD \$29b in 2014 value). The regions of Bío-Bío, La Araucanía, Los Lagos and Los Ríos are shown to suffer the largest losses. The size of the estimated losses underscores the need for proper planning through mitigation to ensure financial recovery.

## 7. Acknowledgement

This work is done using AIR-Worldwide's earthquake model for South America. Development of the model is a result of collaboration between several groups and individuals. The authors would like to thank the Exposure, Seismic Hazard and Tsunami Hazard teams at AIR-Worldwide.

## 8. References

- [1] USGS. Historic Earthquakes Chile 1960 May 22 19:11:14 UTC Magnitude 9.5. The Largest Earthquake in the World. United States Geological Survey. [http://earthquake.usgs.gov/earthquakes/world/events/1960\\_05\\_22.php](http://earthquake.usgs.gov/earthquakes/world/events/1960_05_22.php)
- [2] NOAA (2013). World Data Service (NGDC/WDS): Significant earthquake database. *National Oceanic and Atmospheric Administration*. <http://www.ngdc.noaa.gov/nndc/struts/form?t=101650&s=1&d=1>
- [3] Lazo, R., (2008). Estudio de los Daños de Los Terremotos del 21 y 22 de Mayo de 1960 – *Memoria Para Optar al Título de Ingeniero Civil*. Universidad de Chile.
- [4] Contreras, V. and Boroschek, R., (2012). Strong ground motion attenuation relations for Chilean subduction zone interface earthquakes. *Proceedings of Fifteenth World Conference on Earthquake Engineering*. Lisbon, Portugal.
- [5] Youngs, R. R., Chiou, S.J., Silva, W.J., Humphrey, J.R., (1997). Strong Ground Motion Attenuation Relationships for Subduction Zone Earthquakes. *Seismological Research Letters*, 68, 58-73.
- [6] Atkinson, G. M., and Boore, D.M., (2003). Empirical Ground Motion Relations for Subduction-Zone Earthquakes and their Application to Cascadia and Other Regions. *Bulletin of the Seismological Society of America*, 93, 1703-1729.
- [7] Zhao J. X., Zhang, J., Asano, A., Ohno, Y., Oouchi, T., Takahashi, T., Ogawa, H., Irikura, K., Thio, H., Somerville, P., Fukushima, Y., (2006). Attenuation Relations of Strong Ground Motion in Japan Using Site Classification Based on Predominant Period. *Bulletin of the Seismological Society of America*, 96, 898-913.
- [8] Gregor N. J., Silva, W.G., Wong, I.G., Youngs, R.R., (2002). Ground-Motion Attenuation Relationships for Cascadia Subduction Zone Megathrust Earthquakes based on Stochastic Finite-Fault Model. *Bulletin of the Seismological Society of America*, 92, 1923-1932.
- [9] Vivallos C., J.; Ramírez C.P.; Fonseca H. A., (2010). Microzonificación Sísmica de la Ciudad de Concepción, Escala 1:20.000 No. Mapa: M177. *Carta Geológica de Chile*, Serie Geología Ambiental. SERNAGEOMIN.
- [10] Brantt, C., (2011). Microzonificación sísmica del sector sur poniente de Santiago comunas de Buin y Paine. *Memoria de Título*. Departamento de Geología. Universidad de Chile
- [11] Von Igel G., B., J. A. Naranjo S., and R. Wall Z. 2004. Geología para el ordenamiento territorial de la región metropolitana de Santiago, 2004. Respuesta sísmica de la región metropolitana de Santiago. Escala 1:250.000. No. Mapa: M115.
- [12] Ramirez, P., Vivallos, J., Cáceres, D., Fonseca, A., (2012). Microzonificación Sísmica de la ciudad de San Pedro de la Paz, Región del Bío-Bío. Servicio Nacional de Geología y Minería, Serie Geología Aplicada 16:3 mapas en una hoja, escala 1:20.000. Santiago Naranjo and Carrasco 2010
- [13] Naranjo, J. A. and R. Carrasco, (2010). Zonificación actualizada de la respuesta sísmica de la comuna de San Antonio, Región de Valparaíso. *A report of SERNAGEOMIN*, Chile.
- [14] TUNAMI (Tohoku University's Numerical Analysis Model for Investigation of Near-field tsunamis). Disaster Control Research Center of Tohoku University
- [15] Okada, Y., (1985). Surface deformation due to shear and tensile faults in a half-space. *Bulletin of the Seismological Society of America*, 75, 1135-1154.
- [16] INE, (2001). Anuario de Edificación. Instituto Nacional de Estadísticas. Santiago, Chile.



- [17] Alvarez, C. Rivera, F. Santa Maria, H. Hube, M.A., (2015). Development of an Exposure Model of Residential Structures for Chile. *Proceedings of the Tenth Pacific Conference on Earthquake Engineering*. Sydney, Australia.
- [18] Rossetto, T. and Elnashai, A., (2003). Derivation of Vulnerability Functions for European-type RC Structures Based on Observational Data. *Engineering Structures*, 25: 1241-1263.
- [19] NIST, (2012). Comparison of U.S. and Chilean Building Code Requirements and Seismic Design Practice 1985-2010. *National Institute of Standards and Technology*. U.S Department of Commerce.
- [20] Federal Emergency Management Agency (FEMA) (2012). Seismic Performance Assessment of Buildings, Volume 3: Performance Assessment Calculation Tool (PACT) Version 2.9.65. FEMA P-58-3.1. Washington, D.C.: Department of Homeland Security, FEMA Mitigation Division
- [21] Tapia, P. Roldán, W. Villacis, C., (2002). Vulnerabilidad Sísmica de las Ciudades del Norte de Chile: Arica, Antofagasta y Copiapó. *VIII Jornadas Chilenas de Sismología e Ingeniería Antisísmica*, Chile–2002
- [22] CVC (2005). Microzonificación Sísmica y Estudios Generales de Riesgo en las Ciudades de Palmira, Tuluá y Buga. Corporación Autónoma Regional del Valle del Cauca. Chile.
- [23] Central America Probabilistic Risk Assessment (CAPRA), (2012). Vulnerability Assessment, Basic Concepts. Conference. Thimphu., Bhutan.
- [24] Lai, T., Nasser, A., Katiyar, V., Tang, Y., Guin, J., Towashiraporn, P., (2012). A uniform framework of seismic vulnerability assessment and its application in seismic risk analysis of European countries. *Proceedings of the 15th WCEE*, Lisbon, Portugal 2012.
- [25] Ministry of Land, Infrastructure, Transport, and Tourism (MLIT), (2011), Status survey results affected by the earthquake east, in Japanese. [http://www.mlit.go.jp/report/press/toshi07\\_hh\\_000056.html](http://www.mlit.go.jp/report/press/toshi07_hh_000056.html).
- [26] Reese, S., Bradley, B.A., Bind, J., Smart, G., Power, W., Sturman, J., (2011). Empirical building fragilities from observed damage in the 2009 South Pacific tsunami, *Earth-Science Reviews*, 107:156-173.
- [27] Fan, Y., Li, H., Miguez-Macho, G., (2013). Global patterns of groundwater table depth. *Science*, 339, 940-943, doi:10.1126/science.1229881.
- [28] Holzer, T., H., Noce, T., E., Bennett, M., J., (2011): Liquefaction probability curves for surficial geology. *Environmental & Engineering Geoscience*, 17 (1), 1–21,
- [29] Idriss, I. M. and Boulanger, R.W., (2008). Soil liquefaction during earthquakes. *Monograph MNO-12*, Earthquake Engineering Research Institute, Oakland, California.
- [30] Ishihara, K. and Yoshimine, M., (1992). Evaluation of settlements in sand deposits following liquefaction during earthquakes. *Soils and Foundations*, 32: 173–188.